https://doi.org/10.48048/tis.2022.140

Novel $CaCO_3$-Based Material Formulation for Orange-Colored Spectrum Tracer Projectile

Nining Sumawati Asri[1,*], Abdul Basyir[1], Didik Aryanto[1], Isnaeni[1], Diang Sagita[2], Wahyu Bambang Widayatno[1], Agus Sukarto Wismogroho[1] and Denny Lesmana[3]

[1]Research Center for Advanced Materials, National Research and Innovation Agency, South Tangerang, Banten 15314, Indonesia
[2]Research Center for Appropriate Technology, National Research and Innovation Agency, Subang City, West Java 41213, Indonesia
[3]Ammunition Division, Pindad Ltd. (Persero) General Sudirman Street, Turen, Malang, East Java 65175, Indonesia

([*]Corresponding author's e-mail: nini008@brin.go.id)

Received: 29 October 2021, Revised: 27 December 2021, Accepted: 31 December 2021, Published: 4 November 2022

Abstract

This study underlines the development of orange-colored spectrum tracer material based on Fe/$CaCO_3$/PVC compound. The optimum composition of the compound was determined by comparing three different ratios of Fe-$CaCO_3$-PVC. The sample with the highest $CaCO_3$ content decomposed earlier than that of the other samples. This sample also produced the lowest calorific energy around 275.61 cal/g and emitted a medium-dark orange spectrum. The color brightness was affected by the number of color source materials as well as $CaCl_2$ and $Ca(OH)_2$ which were formed during the combustion process. Meanwhile, the sample with the lowest $CaCO_3$ content produced light orange color with a sharp spectrum emission. The concentration of fuel material (Fe) as well as the higher calorific energy (466.39 cal/g) of this composition contributes to the enhanced spectrum intensity. All samples emitted the orange color, with the wavelength ranging from 585 to 593 nm. Beside of calcite as the main phase, the x-ray diffraction analysis at 650 ℃ shows Fe_2O_3 as a secondary phase. The FTIR analysis of the as-heated sample presents the Fe-O bending band with a broader peak, which can be attributed to the existence of Fe_2O_3 species. The presence of this structure made all these samples have high ignition temperature.

Keywords: Tracer formulation, Calcium carbonate, Iron, Thermal decomposition, Spectrum emission

Introduction

Material science is a multidisciplinary and broad area of research that has increased widely in recent years for many applications. Several of them are developed for the military research field, such as material for the propulsion, warheads, frames in rockets or missiles [1], armor for personal defences or vehicles [2], as well as projectile components in ammunition [3]. One of the important components in the projectile is the tracer material which is added into the backside of the core and frontside of the ignition material. Thus, if the projectile is fired to the target, the tracer will be ignited by the ignition material and then it generates heat energy and luminous color. This kind of tracer is called tracer projectile, which is intended to be the marker of target position [4]. Since the tracer projectile can produce heat energy and spark, it can also be used as an explosive and burn trigger in High-Explosive Incendiary - Armour Piercing (HEI-AP) ammunition [5].

In general, the tracer material is widely produced using pyrotechnic method. Pyrotechnic composition is a heterogeneous mixture of fuel, oxidizer, color source and binder. It consists of either inorganic or organic material ingredients or both of them [6-8]. When suitably ignited, a pyrotechnic composition produces special effects such as light, smoke, heat, delay, sound and pressure depends on the variety of the fuel and oxidizer material [9,10]. Specifically, bright light is preferable for signaling and tracking the projectile. Certain elements and compounds which act as a color source possess the unique property of emitting lines or narrow bands of light in the visible region when they are heated at elevated temperature [11,12]. Some color source materials (e.g. strontium, sodium, barium and copper) have been widely used to generate red, yellow, green and blue colors for tracer material, respectively [13,14]. The color source can also act as the oxidizer and generally come in the form of nitrate, carbonate, chlorite or halocarbon group.

Meanwhile, the typical fuel material can be either metal or non-metal, such as aluminum, magnesium, silicon, carbon-based and many others, which is mixed with either natural or synthetic binder [15,16]. Herein, magnesium is the most used fuel material which is used for many colored light formulas. In the oxidizing flame environment, the metal fuel should converts into metal oxide which emits white light.

There are 2 specific requirements for tracer compounds. The obtained color from the compound must be observable in a specified wavelength region and consider the visual perception of the human observer. Therefore, the tracer with red color is widely used for projectile since the human eye is more sensitive to see red color in dark conditions compared to other colors such as yellow, green and blue [5].

Based on several previous reports related to the trace material and/or pyrotechnic compositions, the primary color is the most popular to be generated. Red color, with the wavelength ranging from 650 to 780 nm, is usually produced using strontium based-compounds such as $Sr(NO_3)_2$ [17], $Sr(OH)_2$, $SrCl_2$ [18]. In another report, the light intensity of the red flare composition could be increased by adding the additive as gas-generated material. Among the investigated additive materials, guanidinium nitrate (GN) showed the best performance to generate a high specific luminosity (Lsp). It found that the Lsp value is comparable to the total amount of oxygen and nitrogen present in the gas generating additive [19]. Further, blue color, with the wavelength ranging from 425 - 500 nm, is commonly generated from copper based-compounds such as $CuCO_3.Cu(OH)_2$ [13], Cu powder electrolytic, basic copper carbonate $Cu_2(CO_3)(OH)_2$, copper benzoate, Paris green, CuOCl, CuO [20] and Cu_3Cl_3 [21]. Juknelevious *et al*. [22], reported the use of the pyrotechnic composition to develop the blue strobe using a formulation called Jennings-White's blue strobe No.5, which could maintain the flame color quality [22]. The formulation contains 55 % ammonium perchlorate (AP), 30 % tetramethylammonium nitrate (TMAN) and 15 % copper, by the less reactive fuels could cause flash frequencies to increase greatly, thus the resulting compositions were either rapidly strobing or constantly ignite. The alternative compositions for blue strobe pellet were also examined by using aminoguanidinium nitrate (AGN) combine with AP and copper as the catalyst. The formulation can produce sharp and well-defined flashes of the blue color, possibly due to the combination of an exothermic reaction and ignition of flammable gases at the surface [23]. While yellow color, with the wavelength ranging from 575 - 600 nm, can be obtained using sodium based-compound [14].

In addition, the secondary color can be generated either by mixing the compound with the respective primary color or by using certain compound which can emit the secondary color. For instance, the green color can be obtained by mixing CuCl, as a blue color source, and sodium based compound, as the yellow color source [24], or by using specific single-component compounds such as $Ba(NO_3)_2$ [25], BaOH, BaCl and CuOH [26].

Orange color, with the wavelength ranging from 590 to 620 nm, possesses the similar characteristics with that of red color in human eye sensibility, yet rarely used as a tracer material. This color can be generated from the calcium based-compounds (e.g. $Ca(OH)_2$ and $CaCl_2$) [26]. Since orange color possess the closest characteristic to the primary red color, it can be used as an alternative for the bright light tracer. Since the tracer material mixture generates luminosity as well as heat energy when it is used as the projectile, further research is required to find the optimum composition in order to avoid excessive heat energy, which can induce the breakage and/or crack to the jacket projectile, affecting the projectile accuracy or even causing injury to the user [5].

The main purpose of this research is to evaluate and find the best material composition which emits intense orange spectrum, while maintaining low calorific energy in order to avoid potential damage to the projectile jacket. Herein, the composition of fuel, oxidizer and binder (i.e. Fe, $CaCO_3$ and PVC) will be optimized to obtain the best composition. Instead of magnesium (Mg), iron (Fe) was used as a fuel since it has lower specific heat capacity and heat of combustion than that of magnesium [9,27-30], which is expected to generate lower heat energy.

Materials and methods

The main constituents of tracer are oxidizer, metal fuel, color source, color intensifier and binder. In this research, $CaCO_3$ (analytical grade) was used as a color source and oxidizer, PVC (technical grade) acts as a binder and color intensifier, while Fe (fine powder of 250 - 350 mesh) acts as a metal fuel. The material formulations used in this research are presented in **Table 1**.

In this study, the tracer material was developed using a simple mechanical grinding technique with careful preparation to ensure sample homogeneity. The thermal properties of the samples were analyzed using thermogravimetric analysis (TGA) (NETZSCH TG 209 F1 Libra type), differential thermal analysis (DTA) (P2F LIPI type) and calorimeter (Parr 1341 Oxygen Bomb Calorimeter type). The TGA and DTA

process was performed at temperature of 37 - 1,000 ℃, with the heating rate of 10 ℃/min at atmospheric environment.

Table 1 Material formulation of the tracer material.

Sample	Fe wt.%	$CaCO_3$ wt.%	PVC wt.%
P1	17	68	15
P2	22	63	15
P3	27	58	15

The material phase was determined using X-Ray Diffraction (XRD) analysis (Rigaku, Smartlab type) with Cu Kα radiation (λ = 1.5418 Å). The functional group of the materials was observed using Fourier Transform Infra-Red (FTIR) (Thermo Scientific, Nicolet iS-10 type) to elucidate the bonding within the compound as well as its potential chemical reactions. The density of the powder samples was also measured using a Pycnometer. In addition, the emission spectral measurement was performed at a dark tunnel with a length of 1 m using Maya2000 Pro series spectrometer, while the samples were burned by Liquefied Butane Fuel tube.

Results and discussion

Thermal properties analysis

In order to understand the thermal phenomenon of this composition during the burning process, the Fe-$CaCO_3$-PVC ternary mixture was analyzed using DTA and TG-DTG analysis. **Figure 1** shows the TG-DTGA and DTA curves of the samples mixture. The three samples possess relatively similar thermal behavior, with a slight intensity difference due to the different mass ratios of each sample.

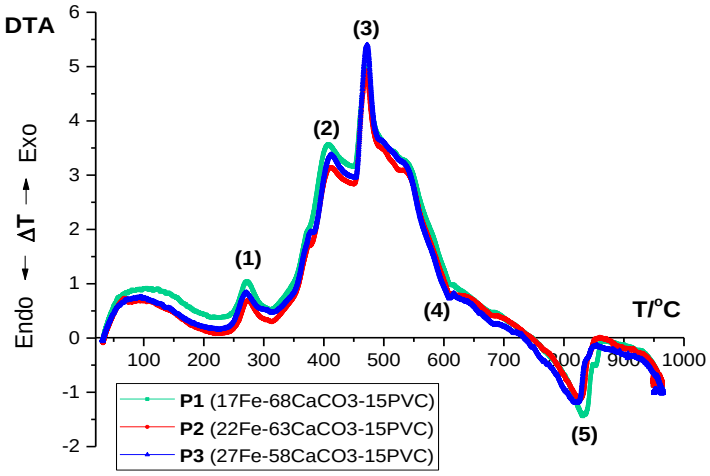

(a)

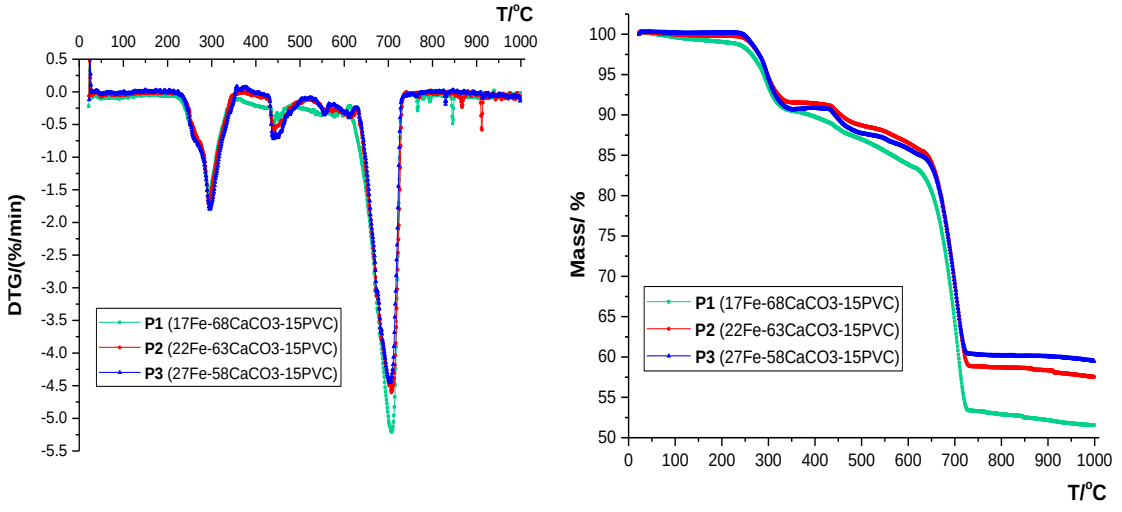

(b) **(c)**

Figure 1 (a) DTA, (b) DTG and (c) TG curves of the mixture containing iron metal powder, calcium carbonate and polyvinyl chloride.

Based on the DTA chart, 5 main peaks are presented in this composition. Peaks 1, 2 and 3 in **Figure 1(a)** indicate the exothermic process, while peak 4 and 5 represent the endothermic process. Peak 1 occurs at around 290 ℃, which indicates the decomposition process of PVC (binder material). The onset temperature of sample P1 for this peak occurs earlier at 234.710 ℃ than that of P2 and P3 sample (243.035 and 245.802 ℃, respectively). Herein, the PVC content of the sample (C_2H_3Cl) experiences dechlorination process, which is one of the possible degradation reactions of PVC [32,33]. The activation enthalpy (ΔH) and entropy (ΔS) of C_2H_3Cl for this reaction is 2.040 and 0.0159 kcal/mol, respectively [31].

$$C_2H_3Cl \rightarrow C_2H_2 + HCl\ (g) \qquad \Delta_{G230\ ^\circ C} = -9.469\ \text{kcal} \qquad (1)$$

After this reaction finished, some parts of Fe were likely to react with HCl, producing $FeCl_3$ (Eq. (2)) which melted at 306 ℃, giving small endothermic shoulder.

$$4/3Fe + 4HCl\ (g) + O_2\ (g) \rightarrow 4/3FeCl_3 + 2H_2O\ (g) \qquad \Delta_{G230\ ^\circ C} = -104.058\ \text{kcal/mol} \qquad (2)$$

Based on thermogravimetry (TG) data, the mass of each sample was reduced to only around 90 % of the initial mass after the first decomposition finished.

The second peak, occurs at around 440 ℃, indicates the release of hydrocarbon [34-36] as the second stage of PVC degradation, which is strongly related to the decomposition of C_2H_2 as shown in Eq. (3). Alternatively, there is also possibility of reaction between C_2H_2 and $CaCO_3$ to form $Ca(OH)_2$ as shown in Eq. (4), prior to the hydrocarbon decomposition. In addition, carbon species is also evolved, which is indicated by the increase of carbon concentration and gradual decrease of chlorine species [37,38]. In the early process of this stage, $FeCl_3$ also reacts with oxygen and generates Fe_2O_3, which is likely to occur at 310 ℃ (i.e. $FeCl_3$ melting point) as shown in Eq. (5). In addition, the Fe oxidation at a lower temperature is started at a temperature of 300 ℃, and this oxidation had happened rapidly at a temperature of 400 ℃ [39]. Therefore, another Fe is oxidized refer to reaction Eq. (6), so that the mass of P3 composition increases almost 1.5 % (**Figure 1(c)**), while the mass of P1 and P2 composition does not enhance significantly, because the percentage of Fe in these compositions are smaller than in P3 composition.

$$C_2H_2 + O_2\ (g) \rightarrow 3/2C + 1/2CO_2\ (g) + H_2O\ (g) \qquad \Delta G_{430\ ^\circ C} = -141.718\ \text{kcal} \qquad (3)$$

$$C_2H_2 + CaCO_3 + 5/2O_2\ (g) \rightarrow Ca(OH)_2 + 3CO_2\ (g) \qquad \Delta G_{310\ ^\circ C} = -272.431\ \text{kcal} \qquad (4)$$

$$4/3FeCl_3 + O_2\ (g) \rightarrow 2/3Fe_2O_3 + 2Cl_2\ (g) \qquad \Delta G_{310\ ^\circ C} = -18.563\ \text{kcal} \qquad (5)$$

$4/3Fe + O_2\ (g) \rightarrow 2/3Fe_2O_3$ $\Delta G_{300\ °C} = -106.326$ kcal (6)

The third exothermic peak occurs approximately at 480 ℃, which is attributed to the chloride absorption by $CaCO_3$ to form $CaCl_2$ [35,36], as can be seen in Eq. (7). In addition, there is a continuous pyrolysis process of the polyene [40], chain scission of carbonaceous backbone from the previous step, and combustion of products [41] that happens in this step.

$CaCO_3 + 2HCl\ (g) \rightarrow CaCl_2 + CO_2\ (g) + H_2O\ (g)$ $\Delta G_{430\ °C} = -16.920$ kcal (7)

The first endothermic at 605 ℃ represents the dissolution of $Ca(OH)_2$, formed in the previous stage. Afterward, the iron oxide compound is found, as shown in Eq. (8), while the remaining carbonaceous species from the previous process [42] and oxidizer material still have not decomposed yet. This finding is different from another experiment for intermetallic material reaction, and where there was a reaction product between Al and Fe in this temperature [43], but based on XRD data (**Figure 2**), it doesn't find the phase from Fe-Ca reaction. This finding is in line with the previous result, where the interaction between Ca and Fe at 650 °C did not form any product [44]. The remaining mass after this process is 83, 86 and 85 % for P1, P2 and P3 composition, respectively. Herein, the mass loss corresponds to the content of $CaCO_3$ within each sample.

$4/3Fe + O_2\ (g) \rightarrow 2/3Fe_2O_3$ $\Delta G_{650\ °C} = -92.148$ kcal (8)

The second endothermic peak at around 825 ℃ indicates the $CaCO_3$ smelting, where $CaCO_3$ begin to decompose at 614.7, 631.0 and 630.8 ℃ for P1, P2 and P3 sample, respectively. Based on the shape of the endothermic curve at DTG, the decomposition proceeds slowly at the beginning and start to increase considerably after 700 ℃. The concentration of Fe species affects the decomposition rate [45], so that the $CaCO_3$ decomposition of P3 sample runs faster than that of P2 and P1. It can be seen at the curve and maximum temperature of this decomposition in each composition, and where the maximum decomposition temperature for P3, P2 and P1 is 702.802, 703.035 and 705.710 ℃, while this decomposition process runs out at a temperature of 730 ℃ and CaO compound forms completely. The possible reaction of $CaCO_3$ decomposition can be seen in Eqs. (9) - (13). Herein, the Gibbs energy value at temperature lower than 890 ℃ is still positive, indicating that the reaction is not likely to occur. Nevertheless, there is report which mentioned the formation of CaO at the temperature higher than 600 ℃ [46], while another research, found that CaO cannot be formed under 700 ℃ [47].

$CaCO_3 \rightarrow CaO + CO_2\ (g)$ $\Delta G_{600\ °C} = +9.965$ kcal (9)

$CaCO_3 \rightarrow CaO + CO_2\ (g)$ $\Delta G_{700\ °C} = +6.440$ kcal (10)

$CaCO_3 \rightarrow CaO + CO_2\ (g)$ $\Delta G_{730\ °C} = +5.391$ kcal (11)

$CaCO_3 \rightarrow CaO + CO_2\ (g)$ $\Delta G_{825\ °C} = +2.097$ kcal (12)

$CaCO_3 \rightarrow CaO + CO_2\ (g)$ $\Delta G_{890\ °C} = -0.133$ kcal (13)

After $CaCO_3$ decomposition, the final residual mass of P1, P2 and P3 are 51.55, 57.53 and 59.49 %, respectively. The mass loss (around 41 - 49 %) can be attributed to the release of carbon dioxide [47,48]. Herein, the thermal stability of the sample correlates with the ability of the material to maintain its properties while experiencing thermal change. Generally, the material is considered to have better thermal stability when it can maintain to have higher residual mass than other samples after getting heat treatment at same temperature range and heating pattern [34]. Furthermore, the sample with better thermal stability possess higher possibility for avoiding the unstable combustion when this sample is ignited, which can minimize damage to the projectile jacket.

X-Ray Diffraction (XRD) analysis

The XRD pattern of P3 after the sample received the heat treatment at 650 ℃ is shown in **Figure 2**. Phase identification analysis using PDXL XRD Rigaku software exhibits multiphase peaks including calcite, hematite and graphite. However, the peaks are dominated by calcite which is known as natural form of $CaCO_3$. The calcite is seen in diffraction peaks (2θ), 23.02, 29.37, 31.40, 35.93, 39.37, 43.12, 47.47, 48.46, 56.51, 57.35, 60.62 and 64.61. The calcite characteristic at 2 theta value 29.37 corresponds to the (hkl) indices (104), which is identified as a trigonal crystal structure with space group R-3c (PDF Card No.04-012-0489). Although this sample got heat treatment in the range of $CaCO_3$ decomposition temperature, the CaO phase does not find in this XRD pattern. It is caused by the maximum temperature of $CaCO_3$ decomposition that is started at a temperature over 700 ℃, while this XRD data is obtained from sample getting heat treatment at temperature 650 ℃.

Furthermore, the other peaks are shown as hematite (Fe_2O_3) generated from the reaction of the iron oxidation. The main peak of hematite is shown in diffraction peak (2θ) value 33.12, which is correlated to the (hkl) indices (104). This hematite type is also identified as trigonal structure (PDF Card No.01-073-8433). Hereinafter, PVC with chemical formula $(C_2H_3Cl)n$ only leaves the carbon (graphite) content which is proved at 2 theta 26.48 correspond to (hkl) indices (002) after heat treatment (PDF Card No.00-056-0159). It is caused by the decomposition temperature of hydrogen chloride which is contained in PVC is much lower than 650 ℃.

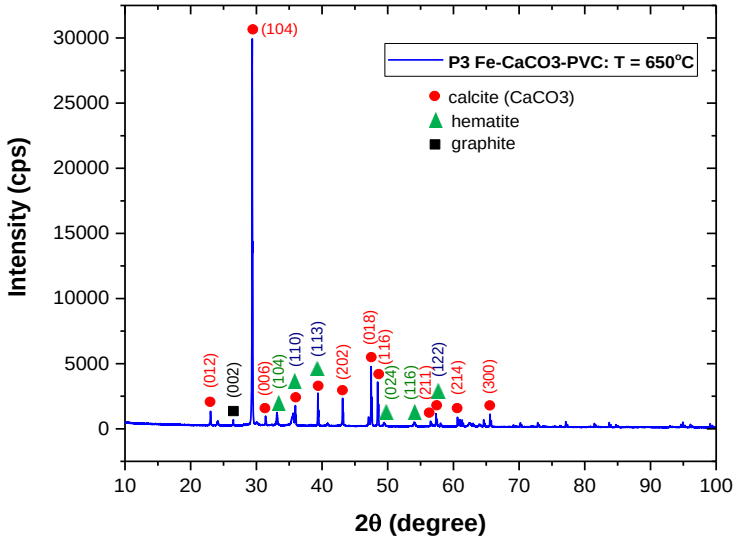

Figure 2 Xray diffraction analysis of P3 after heat treatment at 650 ℃.

Calorimetric and density analysis

The calorie energy indicates the amount of energy generated during the combustion process. To understand the mix composition having calorie energy quantity that is suitable for tracer projectile, the calorimetric analysis also has been done. The material generates high heat energy can cause a crack at the projectile jacket when the ammunition is fired. This will affect the safety of the user as well as the accuracy of the projectile. In other words, the lower heat energy of the tracer projectile composition that is released can avoid and minimize damage to the projectile jacket. **Table 3** shows the calorific value and density of the samples.

Table 3 The calorific energy and density of the samples.

No	Sample	Calorific energy (cal/g)	Density (g/cm^3)
1	P1	275.61	2.24
2	P2	419.84	2.39
3	P3	466.39	2.43

We find that the P3 compound generates the highest result of calorific energy during combustion among the samples prepared. This result depends on the amount of fuel material that is used, which is known as the higher Fe, the total heat energy is released also increase. Besides that, P3 also possesses the highest density, and where higher density or mass generated higher thermal energy [49]. In addition, there is a correlation between density quantity and thermal stability quality of composition, and where the increasing density can produce better thermal stability [50]. It can be seen in the TG data, and where P3 has better thermal stability than P1 and P2. So, although the P3 sample generates the biggest heat energy, this composition has the best thermal stability. Furthermore, the calorific energy value from this composition is still far under the threshold from heat energy required.

The density of this sample is measured using a pycnometer and calculated using the Eq. (14):

$$\rho_s = \frac{(m_3 - m_2)}{[(m_2 - m_1) - (m_4 - m_3)]} \times \rho_l \quad (14)$$

where, ρ_s is the density of the measured sample, ρ_l is the density of liquid media used in the measurement (e.g. water density = 1 g/cm^3), m_1 is the mass of pycnometer, m_2 is the total mass of pycnometer, and liquid media, m_3 is the total mass of pycnometer and powder sample, while m_4 is the total mass of pycnometer which is filled with the liquid media and powder sample.

Fourier Transform Infra-Red (FTIR) analysis

The functional group of the compound was analyzed using FTIR and summarized in **Figure 3**. The spectrum shows the stretching and bending vibration characteristic of the Fe-$CaCO_3$-PVC compound. The lowest wavenumber range from 400 - 600 cm^{-1} is the characteristic of the metal-oxygen (M-O) functional group. The absorption band of $CaCO_3$ is shown at 712 cm^{-1}(v_4), 875 cm^{-1} (v_2) and 1420 cm^{-1} (v_3) which corresponds to the CO_3 bending and stretching vibration band [51,52]. Moreover, the peak at 1,799 cm^{-1} also representing the vibration of the carbonate ions which is common in crystalline polymorphs [53]. In addition, PVC is represented as symmetrical and asymmetrical C-H stretching peaks at 2,511 cm^{-1} and 2,873 cm^{-1}, respectively [54]. Finally, the broad peak at 3429 - 3443 cm^{-1} denotes the -OH stretching vibrating band [53].

Furthermore, the P3 sample receives heat treatment at 650 and 850 ℃ and the functional group composition is shown in **Figure 4**. There is a change of absorption intensity after heat treatment. The intensity band at 3,443 cm^{-1} (-OH stretching) sharply increases after heating at 650 ℃ due to the interaction between calcium carbonate with hydrochloric acid which generates the amount of H_2O, however the peak intensity reduced after the temperature reached at 850 ℃. In addition, there is also a shaper band at 1,625 cm^{-1} (O-H bending), which suggests that there was chemically bound water in the samples [53,55]. On the other hand, the heat treatment at 650 ℃ also leads the slightly shifting vibration peak at 2,512 cm^{-1} into 2,511 cm^{-1}, where this peak is represented as a hydrocarbon chain (C-H). The C-H vibration peak seems disappearing after the sample was heated at 850 ℃. Moreover, the intensity of CO_3 peak in wavenumber of 1,420, 875 and 712 cm^{-1} which shows characteristic absorption bands of calcite also tends to decrease at 650 ℃ and specifically the sym CO_3 vibration band (v_4) disappeared by temperature increase. This phenomenon can be understood refer to TG-DTG data, $CaCO_3$ starts decomposition at a temperature range of 600 - 730 °C. Moreover, the intensity of the Fe-O chain at a wavenumber of 480 cm^{-1} runs into reduction because of the mass degradation of Fe_2O_3 that forms since the temperature of 300 ℃.

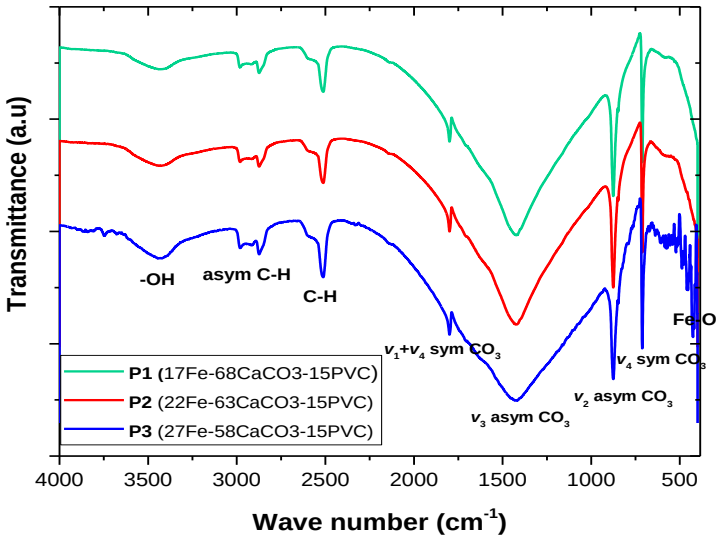

Figure 3 FTIR spectra of P1, P2 and P3 samples.

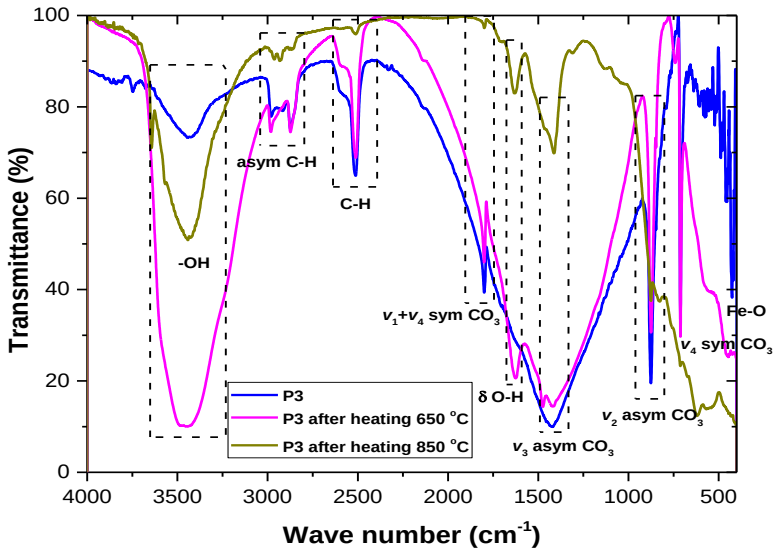

Figure 4 FTIR spectra of P3 after heat treatment at 650 and 850 ℃.

Spectroscopy intensity

Based on a previous study, calcium compounds can emit orange flare at a wavelength of 585 - 620 nm [56]. **Figure 5** shows the spectral emission of Fe-$CaCO_3$-PVC mixture with different compositions. The mixture which contains the highest Fe (P3 composition) emits the sharpest spectrum emission compared to other samples. It can be seen that the spectrum band of this compound has the smallest width. In addition, all samples emit spectrum since the wavelength of 415 nm (**Figure 5(a)**), and where the maximum peak of these spectrums appears at a wavelength around 589 nm (**Figure 5(b)**). This result has good agreement with the previous study [56] which explained the range of the orange spectrum. The presence of Fe as one of the most common materials used as fuel in colored flame composition [57] other than Mg [58] increases strong emission. The differentiated of the color intensity of samples is caused by several reason. The first assumption is due to the amount of heat energy which directly relates to a high number of excited molecules in the flame which result in the orange color of flare is very luminous. The second assumption following the TG-DTG analyzing, where the P3 composition decompose run faster than P1 and P2 at higher temperature. This also related to the amount of fuel (Fe) which consist in the composition. Generally, fast

burning composition result in the lighter, while the slower burning will generate the deep color of flare [19].

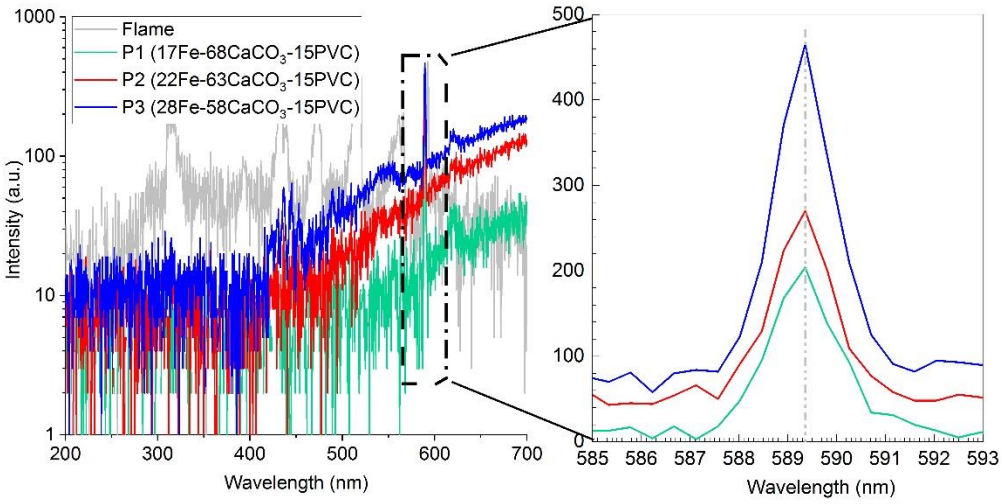

(a) **(b)**

Figure 5 The colored spectrum of P1, P2 and P3 sample (a) at a wavelength of 200 - 700 nm and (b) at a wavelength of 585 - 593 nm

Based on eye view, all these compositions emitted the orange color which is similar (**Figures 6(a) - 6(c)**), only different with the color of butane flame burner (**Figure 6(d)**). However, based on spectrum data of all these compositions which has plotted in a chromaticity diagram (**Figure 7**), it can be seen clearly that P1 emits an orange spectrum darker than others. As the third assumption, it is caused by the $CaCO_3$ percentage in this sample which is the biggest. In addition, based on DTA and TG-DTG data, this material has been decomposed to be $CaCl_2$ and $Ca(OH)_2$. These compounds were known as a material that produced orange flare [6,9,10,57]. Moreover, the P3 composition emits a light orange spectrum because the number of iron percentages in this sample is the highest. This iron emits a yellow spectrum and accelerates the decomposition process of color source material so that can bother and reduce the orange color quality that is produced by $CaCO_3$.

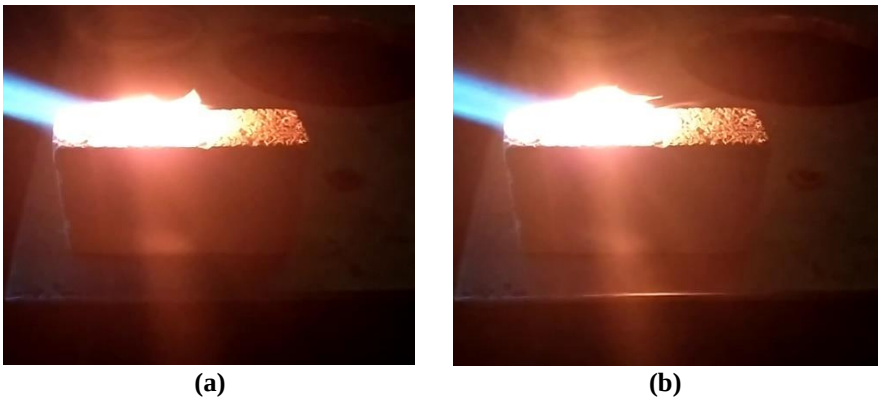

(a) **(b)**

(c) **(d)**

Figure 6 The visual color which emission by (a) P1, (b) P2 and (c) P3 composition after burned by (d) butane flame.

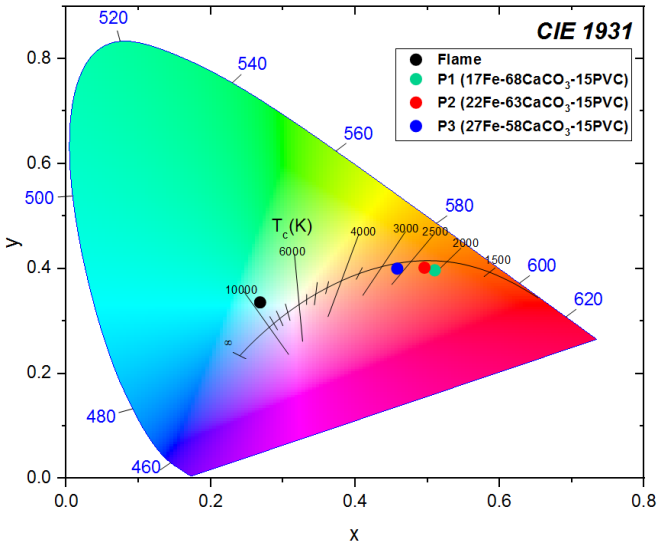

Figure 7 The chromaticity diagram (CIE 1931) of P1, P2 and P3 sample.

To emit the spectrum of this composition has been required a high ignition temperature. It is caused Fe_2O_3 compound that is formed by fuel oxidation during the combustion process, and where this oxidizer has decomposition enthalpy type of endothermic heat [57]. So, to reduce this ignition temperature, this composition has to add or react with active material or energetic fuels such as Al, Mg, Si, Zr or B.

Conclusions

Calcium carbonate ($CaCO_3$) has been found as the potential source of orange-colored flare. Combined with Fe as fuel and PVC as binder and color intensifier, the mixture material exhibit the enhancement of orange-colored flare intensity by increasing the fuel even though with a few color source materials. The tracer samples show good thermal stability which is proved by TG-DTA analysis after heating until 1,000 °C. The calorie energy released while the combustion process is also relatively low, range of 275.61 - 466.39 cal/g, which is needed to avoid damage on jacket projectile by tracer material combustion. The optimum intensity of the orange-colored spectrum is obtained at the composition 27Fe-58$CaCO_3$-15PVC where this sample involves calorific energy of 466.39 cal/g in a combustion process. This composition emitted lighter orange color compared to other samples. The increasing of $CaCO_3$ content in samples ratio will obtain the medium to darker orange spectrum emission. The darkness of this color was affected by the number of color source materials as well as $CaCl_2$ and $Ca(OH)_2$ which were formed during the combustion process. Meanwhile, the sample with the lowest $CaCO_3$ content produced light orange color with a sharp spectrum emission. The quantity of fuel material (Fe) and higher calorific energy (466.39 cal/g) in this composition had a role to enhance the spectrum intensity. The XRD analysis shows a multi-phase after

heating at 650 ℃. The main phase is calcite and the secondary phase is Fe_2O_3. The analysis of functional group of samples also indicates the formation of Fe_2O_3 after heating. The Fe_2O_3 that formed in all this composition made all these samples have a high ignition temperature. This is the main reason of orange flare in this work has not been observed easily, thus it is necessary to improve the composition of the compound.

Acknowledgements

This work was supported by the National Innovation System Research Program (INSINAS) 2020 - 2021 of the Research and Technology Ministry of the Republic of Indonesia (RISTEK-BRIN) with grant number 46/E1/KPT/2020. Besides that, the researcher said thanks to Mr. Ramy Sadek from Polytechnique Montreal for advice and guidance in the synthesis method of this research.

References

[1] AA Vicario, SMS Ramanan, S Arun. Composites in missiles and launch vehicles. *Compr. Compos. Mater.* 2018; **3**, 131-52.
[2] IG Crouch. Body armour - new materials, new systems. *Defence Tech*. 2019; **15**, 241-53.
[3] PJ Hazell. *Armour: Materials, theory, and design.* CRC Press, Boca Rotan, United States, 2016.
[4] J Garner, X Huang, J Mishock and J Kostka. *A tracer analysis for the M1002 training projectile*. U.S. Army Research Laboratory, Maryland, United States, 2009.
[5] A Basyir, NS Asri, D Aryanto, I Isnaeni, C Firdharini, WB Widayatno, AS Sukarto, D Sagita and D Lesmana. Sn-CuO-Arabic gum composition for red tracer projectile ammunition potential. *Jurnal Pertahanan* 2021; **7**, 18-28.
[6] V Lloyd. *Introduction to pyrotechnics.* Research World, New Delhi, India, 2012.
[7] JP Agrawal. *High energy materials: propellants, explosives, and pyrotechnics*. Wiley-VCH, New Delhi, India, 2010.
[8] AA Shidlovsky. *Principles of pyrotechnics.* 3rd ed. American Fireworks News, Pennsylvania, United States, 1997.
[9] KL Kosanke, BJ Kosanke and CJ White. *Lecture notes for pyrotechnic chemistry.* 4th ed. Journal of Pyrotechnics, Wisconsin, United States, 2004.
[10] T Shimizu. *Fireworks: The art, science, and technique*. Pyrotechnica Publications, Texas, United States,1981.
[11] AP Hardt, BL Bush, BT Neyer and T Shimizu. *Pyrotechnis*. Pyrotechnica Publications, Austin, United States, 2001.
[12] SM Buc, G Adelman and S Adelman. *Development of alternate 7.62 mm tracer formulations*. US Army ARDEC, Maryland, United States, 1993.
[13] R Sadek, M Kassem, M Abdo and S Elbasuney. Novel blue flare tracer with enhanced color quality and luminous intensity. *J. Lumin*. 2018; **195**, 8-13.
[14] R Sadek, M Kassem, M Abdo and S Elbasuney. Novel yellow colored flame compositions with superior spectral performance. *Defence Tech*. 2017; **13**, 33-9.
[15] A Bailey and SG Murray. *Explosives, propellants, and pyrotechnics.* Brassey's World Military Technology, London, 1989.
[16] H Ellern. *Military and civilian pyrotechnics*. Chemical Publishing Company, New York, 1968.
[17] R Sadek, M Kassem, M Abdo and S Elbasuney. Spectrally adapted red flare tracers with superior spectral performance. *Defence Tech.* 2017; **13**, 406-12.
[18] D Juknelevicius, L Mikoliunaite, S Sakirzanova, R Kubilius and A Ramanavicius. A spectrophotometric study of red pyrotechnic flame properties using three classical oxidizers: Ammonium perchlorate, potassium perchlorate, potassium chlorate. *Zeitschrift Fur Anorg Und Allg Chemie* 2014; **640**, 2560-5.
[19] D Juknelevicius, P Alenfelt and A Ramanavicius. The performance of red flare pyrotechnic compositions modified with gas generating additives. *Propellants Explos. Pyrotech.* 2020; **45**, 671-9.
[20] D Jukneleviciu, A Hahma, R Webb, TM Klapötke and A Ramanavicius. An experimental comparison of selected blue flame pyrotechnics. *Propellants Explos. Pyrotech*. 2021; **46**, 107-13.
[21] BT Sturman. On the emitter of blue light in copper-containing pyrotechnic flames. *Propellants Explos. Pyrotech*. 2006; **31**, 70-4.
[22] D Juknelevicius, A Dufter, M Rusan, TM Klapötke and A Ramanavicius. Study of pyrotechnic blue strobe compositions based on ammonium perchlorate and tetramethylammonium nitrate. *Eur. J. Inorg. Chem*. 2017; **2017**, 1113-9.

[23] D Juknelevicius, TM Klapötke and A Ramanavicius. Blue strobe pyrotechnic composition based on aminoguanidinium nitrate. *Propellants Explos. Pyrotech.* 2019; **44**, 1466-71.
[24] R Sadek, M Kassem, M Abdo, A Fah, H Tantaw, A Elsaidy and S Elbasuney. Novel colored flames via chromaticity of essential colors. *Defence Tech*. 2019; **15**, 210-5.
[25] D Juknelevicius, R Kubilius and A Ramanavicius. Oxidizer ratio and oxygen balance influence on the emission spectra of green-colored pyrotechnic flames. *Eur. J. Inorg. Chem*. 2015; **2015**, 5511-5.
[26] W Meyerriecks and KL Kosanke. Color values and spectra of the principal emitters in colored flames. *J. Pyrotech*. 2003; **18**, 710-31.
[27] J Carvill. *Thermodynamics and heat transfer*. *Mechanical engineer's data handbook*. Elsevier, Amsterdam, Netherlands, 1994.
[28] AV Grosse and JB Conway. Combustion of metal in oxygen. *Ind. Eng. Chem*. 1958; **50**, 663-72.
[29] I Glassman. *Metal combustion processes*. *Princeton University Aero Engineering Lab*. United States Air Force, New Jersey, United States, 1959.
[30] CE Holley and EJ Huber. *The heat of combustion of magnesium and aluminum*. Los Alamos Scientific Laboratory, New Mexico, United States, 1951.
[31] SS Chang. Heat capacity and thermodynamic properties of poly (vinyl chloride). *J. Res. Nat. Bureau Stand*. 1977; **82**, 9-18.
[32] AR Amer and JS Shapir. Hydrogen halide-catalyzed thermal decomposition of poly (vinyl chloride). *J. Macromol. Sci. A Chem.* 1980; **14**, 185-200.
[33] NS Shuman, MA Ochien, B Sztaray and T Baer. TPEPICO spectroscopy of vinyl chloride and vinyl iodide: Neutral and ionic heats of formation and bond energies. *J. Phys. Chem. A* 2008; **112**, 5647-52.
[34] P Liu, M Zhao and J Guo. Thermal stabilities of poly (vinyl chloride)/calcium carbonate (PVC/$CaCO_3$) composites. *J. Macromol. Sci. B Phys*. 2006; **45**, 1135-40.
[35] VT Lipik, VN Martsul and MJM Abadie. Dehydrochlorination of PVC compositions during thermal degradation. *Eurasian Chem. Tech. J*. 2002; **4**, 25-9.
[36] N Kakuta, A Shimizu, H Ohkita and T Mizushima. Dehydrochlorination behavior of polyvinyl chloride and utilization of carbon residue: Effect of plasticizer and inorganic filler. *J. Mater. Cy. Waste Manag*. 2009; **11**, 23-6.
[37] C Croitoru, C Spirchez, D Cristea, A Lunguleasa, MA Pop, T Bedo, IC Roata and MA Luca. Calcium carbonate and wood reinforced hybrid PVC composites. *J. Appl. Polym. Sci*. 2018; **135**, 46317.
[38] N Dumitrascu, G Borcia and G Popa. Corona discharge treatments of plastified PVC samples used in biological environment. *J. Appl. Polym. Sci*. 2001; **81**, 2419-25.
[39] N Bertrand, C Desgranges, D Poquillon, MC Lafont and D Monceau. Iron oxidation at low temperature (260-500 °C) in air and the effect of water vapor. *Oxid. Met*. 2010; **73**, 139-62.
[40] KP Schlickmann, JLL Howarth, DAK Silva and APT Pezzin. Effect of the incorporation of micro and nanoparticles of calcium carbonate in poly (vinyl chloride) matrix for industrial application. *Mater. Res*. 2019; **22**, e20180870.
[41] XG Li, Y Lv, BG Ma, WQ Wei and SW Jian. Decomposition kinetic characteristics of calcium carbonate containing organic acids by TGA. *Arabian J. Chem.* 2017; **10**, S2534-S2538.
[42] I Bonadies, M Avella, R Avolio, C Carfagna, ME Errico and G Gentile. Poly (vinyl chloride)/$CaCO_3$ nanocomposites: Influence of surface treatments on the properties. *J. Appl. Polym. Sci*. 2011; **122**, 3590-8.
[43] CL Cramer, MS Edwards, JW McMurray, AM Elliott and RA Lowden. Lightweight TiC-(Fe-Al) ceramic-metal composites made in situ by pressureless melt infiltration. *J. Mater. Sci*. 2019; **54**, 12573-81.
[44] NS Martirosyan, T Yoshino, A Shatskiy, AD Chanyshev and KD Litasov. The $CaCO_3$-Fe interaction: Kinetic approach for carbonate subduction to the deep earth's mantle. *Phys. Earth Planet. In*. 2016; **259**, 1-9.
[45] R Font, A Galvez, J Molto, A Fullana and I Aracil. Formation of polychlorinated compounds in the combustion of PVC with iron nanoparticle. *Chemosphere* 2010; **78**, 152-9.
[46] M Bilton, AP Brown and SJ Milne. Investigating the optimum conditions for the formation of calcium oxide, used for CO_2 sequestration, by thermal decomposition of calcium acetate. *J. Phys. Conf. Ser*. 2012; **371**, 012075.
[47] KSP Karunadasa, CH Manoratne, HMTGA Pitawala and RMG Rajapakse. Thermal decomposition of calcium carbonate (calcite polymorph) as examined by in-situ high-temperature X-ray powder diffraction. *J. Phys. Chem. Solid*. 2019; **134**, 21-8.

[48] S Dash, M Kamruddin, PK Ajikumar, AK Tyagi and B Raj. Nanocrystalline and metastable phase formation in vacuum thermal decomposition of calcium carbonate. *Thermochim. Acta* 2000; **363**, 129-35.
[49] AB Bofors. *Analytical methods for powders and explosives*. AB Bofors Nobelkrut, Karlskoga, Sweden, 1974.
[50] NZ Tomic. Chapter 17 - thermal studies of compatibilized polymer blends. *Compat. Polym. Blends* 2020; **2020**, 489-510.
[51] MEI Saraya, H Hassan and A Latif. Preparation of vaterite calcium carbonate in the form of spherical nano-size particles with the aid of polycarboxylate superplasticizer as a capping agent. *Am. J. Nanomater*. 2016; **4**, 44-51.
[52] AZ Noah, MA El Semary, AM Youssef and MA El-safty. Enhancement of yield point at high pressure high temperature wells by using polymer nanocomposites based on ZnO & $CaCO_3$ nanoparticles. *Egypt. J. Petrol*. 2017; **26**, 33-40.
[53] JD Rodriguez-blanco, S Shaw and LG Benning. The kinetics and mechanisms of amorphous calcium carbonate (ACC) crystallization to calcite, viavaterite. *Nanoscale* 2011; **3**, 265-71.
[54] M Pandey, GM Joshi, A Mukherjee and P Thomas. Electrical properties and thermal degradation of poly (vinyl chloride)/polyvinylidene fluoride/ZnO polymer. *Polym. Int.* 2016; **65**, 1098-106.
[55] H Tan, X Zheng, L Chen, K Liu, W Zhu and B Xia. The self-degradation mechanism of polyvinyl chloride-modified slag/fly ash binder for geothermal wells. *Energies* 2019; **12**, 2821.
[56] MS Russell. *The chemistry of fireworks.* Royal Society of Chemistry, Cambridge, 2000.
[57] JA Conkling and CJ Mocella. *Chemistry of Pyrotechnics: Basic Principles and Theory*. 3rd ed. CRC Press, Boca Raton, United States, 2019, p. 225-56.
[58] IM Tuukkanen, EL Charsley, PG Laye, JJ Rooney, TT Griffiths and H Lemmetyinen. Pyrotechnic and thermal studies on the magnesium strontium nitrate pyrotechnic system. *Propellant Explos. Pyrotech*. 2006; **31**, 110-5.